A LATERALLY-IMPLANTED PIEZORESISTIVE SKIN-FRICTION SENSOR

Y. Li, V. Chandrasekharan,, B. Bertolucci, T. Nishida, L. Cattafesta, D.P. Arnold and M. Sheplak
Interdisciplinary Microsystems Group, University of Florida, Gainesville, Florida, USA

ABSTRACT

This paper presents the packaging, fabrication, and calibration of a piezoresistive skin-friction sensor for the direct measurement of wall shear stress. The floating-element structure integrates laterally-implanted piezoresistors into the tether sidewalls to form a fully active Wheatstone bridge for electromechanical transduction. Experimental characterization at a bias voltage of 1.5 V indicates a sensitivity of $4.24\ \mu V/Pa$, a noise floor of 11.4 $mPa/\sqrt{Hz}$ at 1 kHz, a linear response up to the maximum testing range of 2 Pa, and a flat dynamic response up to the testing limit of 6.7 kHz.

INTRODUCTION

The measurement of wall shear stress is of vital importance in a variety of applications. For example, in the design of aerospace and naval vehicles, this measurement provides physical insight into the skin-friction drag distributions, flow separation fronts and transition to turbulent flow. From a scientific perspective, the measurement of the mean wall shear stress, $\overline{\tau}_w$, is essential for the nondimensionalization of a turbulent boundary layer profile via the friction velocity, $u^* = \sqrt{\overline{\tau}_w/\rho}$, where ρ is the fluid density. Moreover, as computing power continues to increase, measurement of fluctuating wall shear stress will be essential for validating direct numerical simulations, a process of considerable value to the turbulence modeling community. Furthermore, since shear stress is a vector field, it may provide advantages over pressure sensing in feedback flow control applications involving separated flows [1]. Unfortunately, the time-accurate, direct measurement of fluctuating shear stress has not yet been fully realized [2]. MEMS–based devices with high-bandwidth and fine spatial resolution capabilities offer the potential to capture physics of the relevant length scales in at least moderate Re flows.

Both thermal and floating element micromachined shear stress sensors have been developed for various flow applications.[2] Thermal devices infer the shear-stress via the measurement of Joulean heating rate, hence calibration for quantitative measurements is difficult. Direct sensors measure the integrated shear force on a floating-element using capacitive, [3-5] piezoresistive,[6, 7] or optical [8-10] transduction schemes. None of these devices have successfully transitioned to wind tunnel measurement tools because of performance limitations and/or packaging impracticalities [2]. For use in a wind tunnel, the sensor package must be flush mounted in an aerodynamic model, robust enough to tolerate humidity variations and immune to electromagnetic interference (EMI). We have attempted to address these limitations via the development of a side-implanted piezoresistive sensor. Figure 1 illustrates the floating element device and the junction-isolated sidewall implanted p-type silicon piezoresistors.

The physical structure consists of a $50\ \mu m$ thick, $1\ mm \times 1\ mm$ element suspended by four $1\ mm$ long, 30 μm wide and $50\ \mu m$ thick tethers. The shear force on the element induces a mechanical stress field in the tethers and thus a resistance change. The piezoresistors are arranged in a fully-active Wheatstone bridge to ideally provide rejection to common mode disturbances, such as pressure fluctuations. A dummy bridge located next to the sensor is used for temperature corrections. The device modeling and design have been previously reported [11].

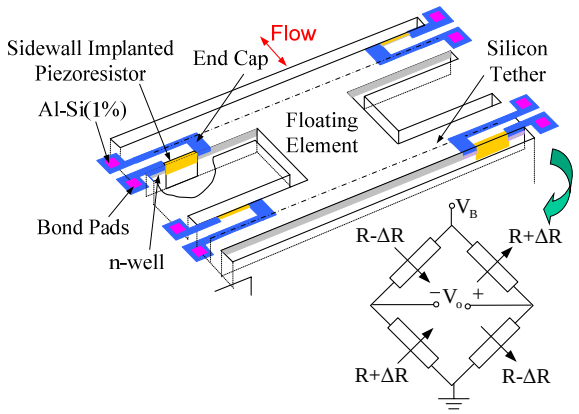

Figure 1: A 3D schematic of the side-implanted piezoresistive shear-stress sensor and equivalent Wheatstone bridge.

FABRICATION AND PACKAGING

In this section, a brief overview of the main sensor fabrication process is given. A discussion of the sensor package and associated interface circuit follows.

The device is fabricated from a SOI wafer using an 8-mask process. A detailed description of the fabrication process development has previously been reported [12]. The process begins with a phosphorus blanket implantation that forms an n-well. Boron implantation forms a heavily doped Ohmic contact. The tethers and floating element are defined by patterning PECVD oxide via RIE (Figure 2 (A)). The patterned Si is etched vertically 8 µm via DRIE to form the trench for the sidewall implant. The scallops formed on the sidewalls during DRIE are smoothed by hydrogen annealing. A 100 nm thick oxide layer is thermally grown as a thin implant oxide on the sidewall. After a preamorphization implant, boron is implanted at an oblique angle of 54˚ to achieve a 5 µm shadow side-wall implantation (Figure 2 (B)). The oxide on the sidewall is etched via BOE, followed by a boron drive-in process to form the piezoresistors. A thin oxide layer is thermally grown as a passivation layer. The tether is defined via DRIE using the BOX layer as an etch stop (Figure 2 (C)). After trench filling with photoresist, the oxide is patterned and etched via BOE to open contact vias, followed by 1 µm thick Al-Si(1%) metallization layer. The metal layer is patterned and RIE etched to form the metal contacts. A PECVD silicon nitride layer is then deposited and RIE etched to expose the bond. The structure is released from the backside using DRIE and RIE (Figure 2 (D)). Finally, the sensors are annealed in forming gas for noise floor improvement. An optical photograph of the fabricated device is shown in Figure 3.

After fabrication, the individual die ($6.2\ mm \times 6.2\ mm$) were separated and then packaged in a printed circuit board (PCB) ($20\ mm \times 20\ mm$). Figure 4 illustrates the sensor die embedded in the printed circuit board and sealed with glue at the perimeter, which in turn is flush-mounted in a Lucite package for easy wind-tunnel mounting. An interface circuit board was designed for offset compensation. This board includes two sets of

compensation circuitry: one for the active bridge and another for the dummy bridge. This board is attached on the backside of the device package and supported by two screws connected to the Lucite package. The copper wires for the signal output or voltage supply in the device package are soldered to the PCB feedthrough vias.

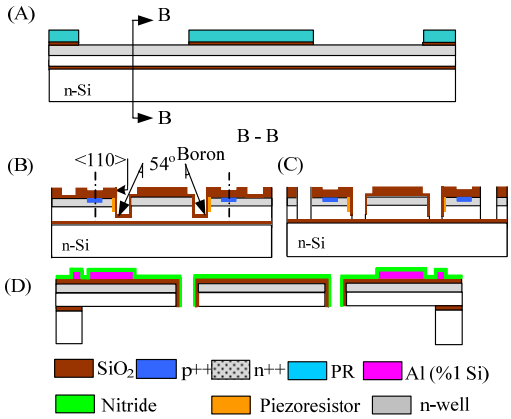

Figure 2: Process flow to fabricate the shear stress sensor.

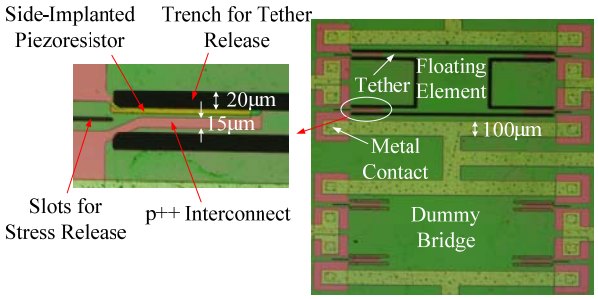

Figure 3: An optical photograph of the fabricated device with a close up view of the tether and side-implanted piezoresistor.

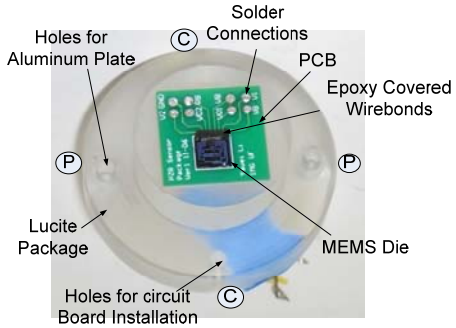

Figure 4: An optical photograph of the sensor package.

EXPERIMENTAL RESULTS

The experiments were performed in the Interdisciplinary Microsystems Laboratory at the University of Florida. Several tests were performed to determine the electrical and shear stress transduction properties.

Electrical Characterization

After fabrication, wafer-level electronic testing of the bridge resistance and junction isolation was conducted using an Agilent 4155C semiconductor parameter analyzer and a wafer level probe station. The leakage current is less than $0.1\,\mu A$ up to a reverse bias voltage of -10 V (Figure 5), after that point a soft break down initiates at -20V (Figure 6). The input and output resistances of the bridge are $414\,\Omega$ and $397\,\Omega$ (Figure 7), respectively.

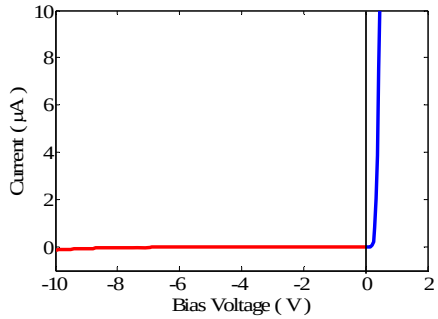

Figure 5: The forward and reverse bias characteristics of p/n diode illustrating the junction isolation of the Wheatstone bridge.

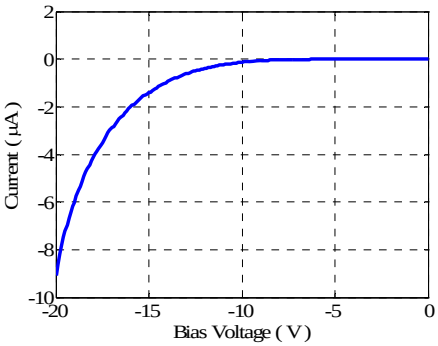

Figure 6: I-V characteristics of the Wheatstone bridge illustrating the breakdown voltage of the p/n diode.

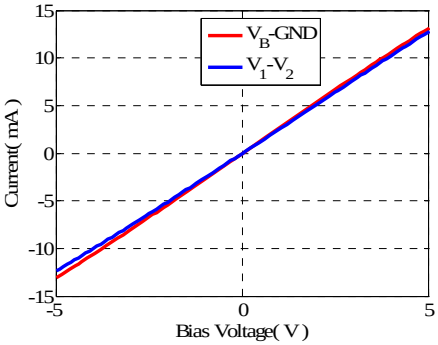

Figure 7: The I-V characteristics of the Wheatstone bridge to extract the input and output resistance.

Dynamic Characterization

The frequency response and linearity were educed using Stokes' layer excitation of shear-stress in a plane-wave tube (PWT). This technique utilizes acoustic plane waves in a duct to generate known oscillating wall shear stresses [13]. A conceptual schematic of the dynamical calibration setup is shown in Figure 8. The plane wave is generated by a BMS 4590P compression driver that is mounted at one end of the PWT. The PWT consists of a rigid-wall 1"x1" duct with an anechoic termination (a 30.7" long fiberglass wedge), which supports acoustic plane progressive waves propagating along the duct. The sensor and a reference microphone (B&K 4138) are flush-mounted at the same axial position from the driver. The usable bandwidth for plane waves in the PWT is determined by the cut-on frequency of the first higher order mode and is $6.7\,kHz$ in air and $20\,kHz$ in helium. The compensated output voltage from the interface circuit is ac-coupled

and amplified 46 dB by SR560 low noise preamplifier. A B&K PULSE Multi-Analyzer System (Type 3109) is used as the microphone power supply, data acquisition unit, and signal generator for the source signal in the plane wave tube.

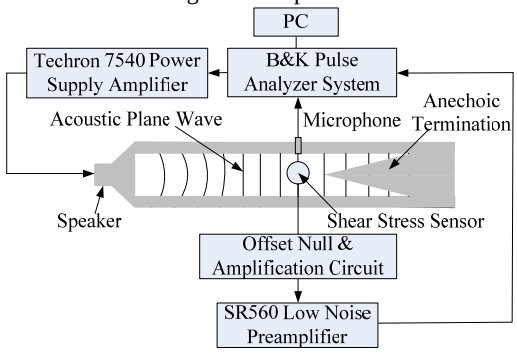

Figure 8: Schematic of experimental setup for the sensor characterization via Stokes' layer excitation.

The dynamic sensitivity and linearity of the sensor was tested with a single tone of 2088 *Hz* as a function of increasing sound pressure levels (SPL) in air. The sensor was operated at bias voltages of 1.0V, 1.25V, and 1.5V. This is substantially lower than the optimized bias voltage of 10 V to avoid resistor self-heating [11]. Any resistor self-heating will lead to temperature-resistive voltage fluctuations due to unsteady convective cooling [14]. The acoustically-generated wall shear stress for the frequency range of excitation in this paper is approximated by [13]

$$\tau'_{wall} = \frac{p'\sqrt{j\omega\nu}}{c} e^{j\left(\omega t - kx - \frac{\pi}{2}\right)} \tanh\left(\sqrt{\frac{j\omega b^2}{\nu}}\right), \qquad (1)$$

where p' is the amplitude of the acoustic perturbation, $j=\sqrt{-1}$, ν is the kinematic viscosity, ω is the angular frequency, $k=\omega/c$ is the acoustic wave number, and b is the duct width.

By adjusting the SPL from 123*dB* to 157*dB*, the induced shear stress varies from 0.04 *Pa* to 2.0 *Pa*. Figure 9 shows normalized output voltages at bias voltages of 1.0 V, 1.25 V and 1.5 V in response to the shear stress variation. The normalized sensitivity is defined as the ratio of the normalized differential sensor output voltage (output voltage/bias voltage) to the input wall shear stress. For all bias conditions, the sensor responds linearly up to 2.0 *Pa* and the normalized sensitivities (slopes of the plots) are 2.905 $\mu V/V/Pa$, 2.882 $\mu V/V/Pa$ and 2.828 $\mu V/V/Pa$, respectively. The predicted normalized sensitivity is 3.65 $\mu V/V/Pa$. For a balanced Wheatstone bridge without resistor self-heating, the normalized sensitivity should be constant. If resistor self-heating occurs, a power-law dependence on the power dissipation is expected. The close match in normalized sensitivities (<3% variation) indicates that the sensor is responding solely to the integrated shear force fluctuations and not unsteady convective cooling.

The frequency response at bias voltage of 1.5 *V* is also investigated in this experiment. The normalized frequency response function of the shear stress sensor is given as [13]

$$H(f) = \frac{V(f)}{\tau_{wall}(f)} \frac{\partial \bar{\tau}}{\partial \bar{V}}, \qquad (2)$$

where $V(f)$ is the sensor output with a known input, $\tau_{wall}(f)$ is obtained via Equation (1), and $\partial\bar{\tau}/\partial\bar{V}$ is the static sensitivity. For this experiment, we normalized with the 2.088 *kHz* sensitivity. Figure 10 demonstrates the magnitude and phase of the actual frequency response function of the shear stress sensor for a nominal input shear-stress magnitude of 0.3 *Pa*. The gain factor is flat and is between −3.01 *dB* to 0.09 *dB* for this test. The phase is flat up to 4.552 *kHz*. These results are not corrected for non-idealities in the anechoic termination which result in finite reflected waves [13]. In addition, there is some suspicion that the results above 4.552 kHz may be corrupted by the scattered evanescent field near the termination. Regardless, there is no apparent resonance in this sensor up to 6.7 *kHz*. Future experiments will be conducted in helium to obtain the resonant frequency.

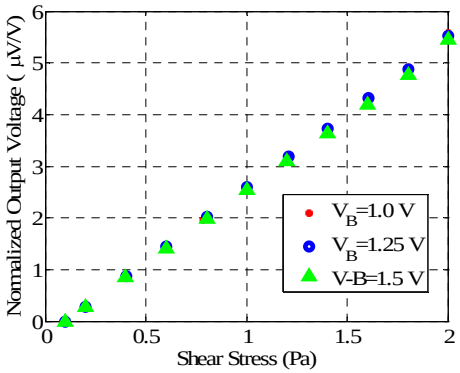

Figure 9: The normalized sensitivity at forcing frequency of 2088Hz with different bias voltages.

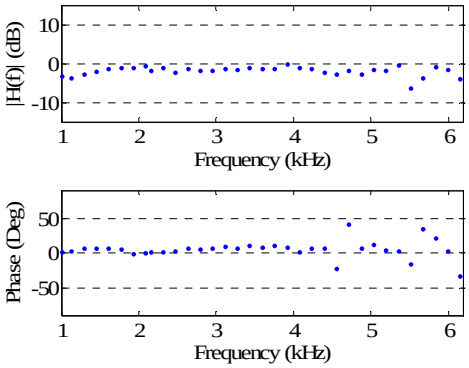

Figure 10: Magnitude and phase of the frequency response function at bias voltage of 1.5V.

Noise Measurement

The lower end of the dynamic range of the sensor is ultimately limited by the device noise floor. This measurement is made by mounting the sensor in the sidewall of the plane wave tube with the speaker amplifier turned off. This provides a reasonable estimate of the entire sensor system noise floor as installed in a calibration chamber. The compensated voltage output is amplified by the SR560 low noise preamplifier (ac coupled), and then fed into the SRS785 spectrum analyzer [14]. The spectrum analyzer measures the noise power spectral density (PSD), using a Hanning window to avoid the PSD leakage. The measured noise PSD includes the sensor noise and the setup noise, such as EMI, noise of amplifier, the spectrum analyzer and power supply. LabView is used for data acquisition and manipulation. The measured output-referred electrical voltage noise floor is shown in Figure 11 for a bias voltage of 1.5 V. As expected, the electronic noise spectrum is dominated by $1/f$ noise indicating

that the signal-to-noise ratio for this sensor is a strong function of frequency. At $1\,kHz$ (with $1\,Hz$ bin) the noise floor is $48.2\,nV/\sqrt{Hz}$ which corresponds to minimum detectable shear stress of $11.4\,mPa$.

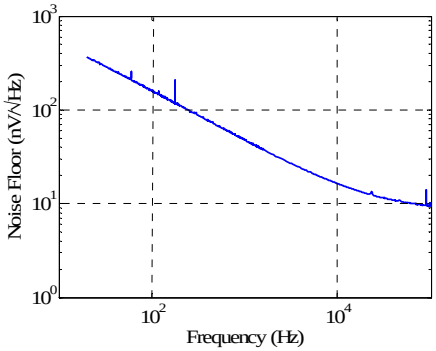

Figure 11: Noise floor of the measurement system.

CONCLUSION

A proof-of-concept micromachined, floating element shear-stress sensor was developed that employs laterally-implanted piezoresistors. A dynamic characterization of the device revealed a linear response up to 2.0 Pa and a flat response up to the frequency testing limit of $6.7\,kHz$. The theoretically predicted resonant frequency is $9.8\,kHz$. Noise floor measurements indicate that $1/f$ noise dominates and a minimum detectable shear stress of $11.4\,mPa$ at $1\,kHz$. Therefore, the experimentally determined dynamic range is $11\,mPa - 2\,Pa$. The theoretically predicted upper end of the dynamic range at 3% static non-linearity is 5 Pa. The upper ends of the dynamic range and bandwidth, however, could not be verified due to constraints in our calibration apparatus. A summary of the experimental results compared to the theoretical results for a bias voltage of 1.5 V are listed in Table 1. The normalized sensitivity is close to the predicted design value, but resistor heating precluded using higher bias voltages thus lowering the maximum allowable sensitivity by $16.5\,dB$. Furthermore, the noise floor is roughly a factor of 7 higher than predicted. This may be because the measured noise floor is the total system noise, which includes setup noise and sensor noise, whereas the predicted value is just due to the sensor and the SR560 preamplifier. There are also substantial differences in the predicted versus realized bridge impedance which means that the voltage noise of the resistors may also be higher than predicted. Isolated measurements of the resistors must be made to quantify this noise source [15].

Table 1: Performance comparison

Parameters	Predicted Value	Experimental Results
Normalized Sensitivity $(\mu V/V/Pa)$	3.65	2.83
Noise Floor (nV)	6.5	48.2
MDS (mPa)	1.2	11.4
Bandwidth (kHz)	9.8	> 6.7
Resistance (Ω)	1000	397
τ_{max} (Pa)	5	>2

REFERENCES

[1] M. Sheplak, L. Cattafesta, and Y. Tian, "Micromachined Shear Stress Sensors for Flow Control Applications," in Proceedings of the IUTAMM Symposium Held at the Royal Geographical Society, London, England 2007.

[2] J. W. Naughton and M. Sheplak, "Modern Development in Shear Stress Measurement," Prog. Aerosp. Sci., Vol. 38, pp. 515-570, 2002.

[3] M. A. Schmidt, R. T. Howe, S. D. Senturia, and J. H. Haritonidis, "Design and Calibration of a Micromachined Floating-Element Shear-Stress Sensor," IEEE Trans. Electron Devices, Vol. 35, pp. 750-757, 1988.

[4] T. Pan, D. Hyman, and M. Mehregany, "Microfabricated Shear Stress Sensors, Part 1:Design and Fabrication," AIAA J., Vol. 37, pp. 66-72, 1999.

[5] J. Zhe, V. Modi, and J. Kenneth. R. Farmer, "A Microfabricated Wall Shear-Stress Capacitative Sensing," J. Microelectromech. Syst., Vol. 14 (1), pp. 167-175, Feb. 2005.

[6] J. Shajii, K.-Y. Ng, and M. A.Schmidt, "A Microfabricated Floating Element Shear Stress Sensor Using Wafer-bonding Technology," J.Microelectromech. Syst., Vol. 1 (2), pp. 89-94, June 1992.

[7] A. A. Barlian, S.-J. Park, V. Mukundan, and B. L. Pruitt, "Design and characterization of microfabricated piezoresistive floating element-based shear stress sensors," Sensors and Actuators A, Vol. 134 (1), pp. 77-87, Feb 2007.

[8] A. Padmanabhan, H. Goldberg, K. D. Breuer, and M. A.Schmidt, "A Wafer-Bonded Floating-Element Shear Stress Microsensor with Optical Position Sensing by Photodiodes," J.Microelectromech. Syst., Vol. 5 (4), pp. 307-315, 1996.

[9] F.-G. Tseng and C.-J. Lin, "Polymer MEMS-Based Fabry–Perot Shear Stress Sensor," IEEE Sensors J, Vol. 3, pp. 812-817, Dec. 2003.

[10] S. Horowitz, T.-A. Chen, V. Chandrasekaran, K. Tedjojuwono, L. Cattafesta, T. Nishida, and M. Sheplak, "A Micromachined Geometric Moiré Interferometry Floating-Element Shear Stress Sensor," in IEEE Solid-State Sensor and Actuator Workshop, 2004, pp. 13-18.

[11] Y. Li, M. Papila, T. Nishida, L. Cattafesta, and M. Sheplak, "Modeling and optimization of a side-implanted piezoresistive shear stress sensor," in Proceeding of SPIE 13th Annual International Symposium on Smart Structures and Materials, San Diego, CA, 2006. Paper No. 6174-7,

[12] Y. Li, T. Nishida, D. P. Arnold, and M. Sheplak, "Microfabrication of a wall shear stress sensor using side-implanted piezoresistive tethers," in Proceeding of SPIE 14th Annual International Symposium on Smart Structures and Materials, San Diego, CA, 2007, pp. Paper No.6529-13.

[13] V. Chandrasekaran, A. Cain, T. Nishida, L. N. Cattafesta, and M. Sheplak, "Dynamic calibration for thermal shear-stress sensors with mean flow," Exp Fluids, Vol. 39, pp. 56-65, 2005.

[14] T. V. Papen, H. Steffes, H. D. Ngo, and E. Obermeier, "A micro surface fence probe for the application in flow reverse area," Sensors and Actuators A, Vol. 97-98, pp. 264-270, 2002.

[15] R. Dieme, G. Bosman, M. Sheplak, and T. Nishida, "Source of excess noise in silicon piezoresistive microphones," J. Acoustical Society of America, Vol. 119, pp. 2710-2720, May 2006.